Tetrahedron Chem 10 (2024) 100064

Contents lists available at ScienceDirect

Tetrahedron Chem

journal homepage: www.journals.elsevier.com/tetrahedron-chem

A molecular electron density theory study of hydrogen bond catalysed polar Diels–Alder reactions of α,β-unsaturated carbonyl compounds

Luis R. Domingo [a,*], Patricia Pérez [b], Mar Ríos-Gutiérrez [a], M. José Aurell [a]

[a] Department of Organic Chemistry, University of Valencia, Dr. Moliner 50, 46100, Burjassot, Valencia, Spain
[b] Universidad Andrés Bello, Facultad de Ciencias Exactas, Departamento de Ciencias Químicas, Centro de Química Teórica & Computacional, Av. República 275, 8370146, Chile

ARTICLE INFO

Keywords:
Diels-Alder reactions
Hydrogen bonds
Catalysis
Stereoselectivity
Molecular electron density theory

ABSTRACT

The hydrogen bond (HB) catalysed Diels-Alder (DA) reactions of acrolein with cyclopentadiene have been investigated within the Molecular Electron Density Theory (MEDT) at the ωB97X-D/6-311G(d,p) computational level. The formation of HBs increases the electrophilicity of these species, suggesting an acceleration of these polar Diels-Alder (P-DA) reactions with forward electron density flux. Formation of one or two HBs with acrolein decreases the activation energies of the HB-catalysed P-DA reactions by 1.7 (methanol) and 4.0 (squaramide) kcal·mol^{-1}, with the corresponding DA reactions exhibiting low *endo* stereoselectivity. These HB-catalysed DA reactions proceed through non-concerted one-step mechanisms via asynchronous transition state structures (TSs). An Interacting Quantum Atoms (IQA) energy partitioning analysis of the TSs indicates that the intra-atomic stabilization of the acrolein framework, coupled with the increase of the global electron density transfer, plays a crucial role in reducing the activation energies of these HB-catalysed DA reactions.

1. Introduction

The Diels-Alder (DA) reaction, first reported by Diels and Alder in 1928 [1], is one of the most important organic reactions from both a synthetic and theoretical point of view [2–4].

In 1969, Woodward and Hoffmann proposed the "pericyclic mechanism" for the DA reaction between butadiene **1** and ethylene **2** [5], but this reaction does not take place easily experimentally (see Scheme 1) [6].

After finding the decisive role of the global electron density transfer [7] (GEDT) taking place at the transition state structures (TS) in the feasibility of DA reactions, the mechanism of the polar DA (P-DA) reactions [8], in which the favourable nucleophilic/electrophilic interactions taking place at the TSs are responsible for the feasibility of the reaction, was established in 2009. After that, the analysis of the electrophilicity [9] ω and nucleophilicity [10] ***N*** indices has become a powerful tool for experimental organic chemists to analyse DA reactions [11,12]. A classification of the DA reactions as non-polar DA (N-DA) reactions with a negligible GEDT lower than 0.1 e, P-DA reactions, and ionic DA (I-DA) reactions was proposed (see Fig. 1). [8].

Even though acrolein **5** is classified, within the electrophilicity scale [11], as a strong electrophile, ω = 1.84 eV, the corresponding DA reactions demand the participation of Lewis acid (LAs) catalysts such as BH_3 or $AlCl_3$ to the reaction takes place easily (see activation energies of the DA reactions of Cp **4** with acrolein **5** and with the acrolein:LA complexes **7** (BH_3) and **8** ($AlCl_3$) in Fig. 1) [8], a behaviour that is readily anticipated by examining the electrophilicity ω indices of the corresponding LA complexes; 3.28 (**7**, BH_3) and 4.62 (**8**, $AlCl_3$) eV [8,13].

In general, P-DA reactions are carried out in polar aprotic solvents such as dichloromethane, but protic solvents such as ethanol, and even water, can be used as well. In 1994, Jorgensen et al. investigated solvent effects on the so-called "pericyclic reactions" by computer simulations [14]. They concluded that the origin of the pronounced acceleration of DA reactions in water was found to involve a significant component from enhanced hydrogen bond (HB) to heteroatoms in the TSs.

In 2002, Huang and Rawal reported the HB-promoted hetero DA reactions involving unactivated ketones [15]. They observed a significantly higher chloroform reaction rate compared to other aprotic organic solvents in the reaction between the*p*-anisaldehyde **9** and the 1-amino-3-siloxy-1,3-butadiene **10** (see Scheme 2). The relative rate coefficients observed for the DA reaction in various solvents did not exhibit a correlation with solvent dielectric constants. For example, the reaction proceeded 10 times faster in chloroform compared to the more polar solvent acetonitrile. These authors concluded that the augmented

* Corresponding author.
E-mail address: luis.domingo@uv.es (L.R. Domingo).

https://doi.org/10.1016/j.tchem.2024.100064
Received 20 December 2023; Received in revised form 1 February 2024; Accepted 12 February 2024
Available online 22 February 2024

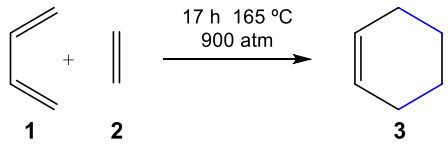

Scheme 1. DA reaction between butadiene **1** and ethylene **2**.

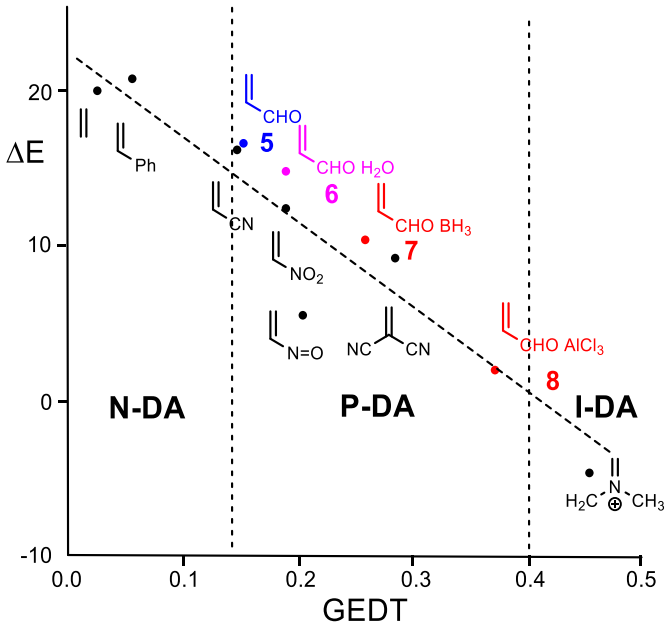

Fig. 1. Plot of the activation barriers (ΔE in kcal·mol^{-1}) vs. the GEDT, in average number of electrons, e, for the DA reactions of cyclopentadiene (Cp) **4** with the substituted ethylene series of increased electrophilic character, $R^2 = 0.89$. The classification of the DA reactions, based on the GEDT, is included.

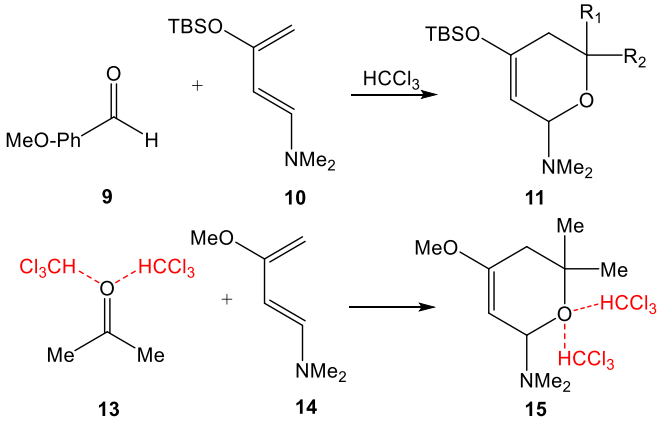

Scheme 2. P-DA reaction of carbonyl compounds accelerated in chloroform.

reaction rate in chloroform might be attributed to a C–H ····O=C interaction, which enhances the electrophilic character of the carbonyl group, thereby rendering it a stronger heteroethylene.

Later, in 2003, Domingo and Andrés theoretically studied the enhanced reactivity of carbonyl compounds in chloroform [16]. That study emphasized that the formation of two non-classical HBs between the carbonyl oxygen of acetone **12** and the hydrogen atom of chloroform accelerated the corresponding P-DA reaction towards the nucleophilic 1-amino-3-methoxy-1,3-butadiene **14** (see Scheme 2). The increase in the GEDT at the corresponding solvated TS, ΔGEDT = 0.04 e, accounted for the acceleration found in this P-DA reaction, $\Delta\Delta H_{act} = -10.8$ kcal mol^{-1}. This behaviour agreed with the increase of the electrophilicity ω index of the solvated acetone **13**; ω = 0.95 eV for acetone **12**, and ω = 1.58 eV for solvated acetone **13**.

Interestingly, among the substituted ethylene series used in Fig. 1, the water-acrolein complex **6** was considered [8]. Formation of an HB between the carbonyl oxygen of acrolein **5** and a hydrogen atom of water accelerated the P-DA reaction, decreasing the activation energy by 2.8 kcal mol^{-1} as a consequence of the increase of the GEDT at the water explicitly solvated TS, ΔGEDT = 0.05 e. This behaviour was again in agreement with the increase of the electrophilicity ω index of water solvated acrolein **6**, ω = 2.04 eV, compared to that of acrolein 5, ω = 1.84 eV.

Recently, Hamlin et al. studied the origin of stereoselectivity and rate enhancement in the catalysed DA reaction of Cp **4** with acrolein **5** by the formation of two HBs with bifunctional HB donors such as urea **16** and thiourea **17** (see Scheme 3) [17]. These authors found that thioureas evidence *exo* selectivity in the studied DA reactions and significantly accelerate the reactions by reducing the barrier by up to 7 kcal mol^{-1}. Using the activation strain model [18] (ASM), these authors concluded that "the rate enhancement provoked by the HBs is exclusively caused by a diminished two-centre four-electron Pauli repulsion between the occupied π-orbitals of Cp and HB-A reactants" [17]. They also established that the exceptional *exo* selectivity computationally obtained in these HB-catalysed DA reactions is directly related to the more considerable degree of asynchronicity along this reaction pathway, leading to the alleviation of destabilizing activation strain and Pauli repulsions.

However, ASM [18] and, consequently, the interpretations that arise from it, have shown to be prone to flaws due to the process dependency of their energy components [19,20]. This means that ASM energy terms, including Pauli repulsions, are not uniquely defined and can be controlled at will to obtain a desired result. Moreover, these arbitrary terms are obtained from unrealizable states of the system that, just as Bader severely criticized, "violate all of the rules of physics, in particular the Pauli principle" [21].

The Molecular Electron Density Theory [22] (MEDT), which proposes that changes in electron density along a reaction, and not molecular orbital interactions, are responsible for the chemical reactivity in organic chemistry, was proposed in 2016. MEDT rejects any outdated model based on MOs such as the Frontier Molecular Orbital (FMO) theory [23] and Morokuma-based energy decomposition schemes [24, 25]. In the MEDT studies a wide range of quantum chemical tools that allow the analysis of density functions, such as the reactivity indices defined within DFT [12,13,26], the electron localization function [27] (ELF), the bonding evolution theory [28] (BET), the quantum theory of atoms in molecules [29,30] (QTAIM) and the non-covalent interaction [31] (NCI), are used.

In 2005, Blanco et al. developed a parameter-free and reference-free energy decomposition scheme based on QTAIM, called Interacting

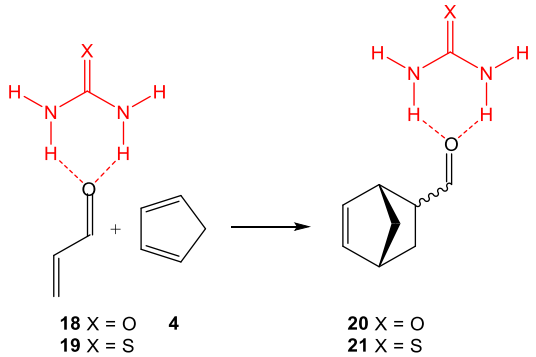

Scheme 3. HB-catalysed DA reactions promoted by urea **16** and thiourea **17**.

Quantum Atoms [32] (IQA). IQA divides the total energy of a system into intra- and interatomic contributions of different nature, which are related to chemical concepts of bonding. More recently, in 2017 Thacker et al. developed the Relative Energy Gradient [33] (REG) method which systematically inspects the correlation between each partitioned energy term and the total energy of the system. REG then ranks all correlations, one for each atomic energy term, in an automated fashion to determine the subset that best describes the behaviour of the total system as it goes through its change. The combination of both IQA and REG can help discerning the origin of reaction barriers [33]. Indeed, IQA-REG has already been successfully applied to a wide variety of interactions and phenomena [34–36], proving itself to be an indispensable, minimal but powerful and general method in the chemist's toolbox for mechanistic studies.

Herein, a complete MEDT study of the HB-catalysed P-DA reactions of α,β-unsaturated carbonyl compounds is carried out to establish how the formation of one or two HBs of hydrogen donor molecules enhances the reaction rate of P-DA reactions. To this end, the DA reactions of Cp **4** with acrolein **5** in the explicit presence of solvent molecules such as methanol, water, trifluoromethanol, or chloroform, i.e. the hydrogen-bonded molecular complexes (HBMCs) **22**, **6**, **23** and **24**, respectively, and in the presence of the bifunctional HB donor molecules urea **16**, thiourea **17** and squaramide **25**, i.e. HBMCs **18**, **19** and **26** in Scheme 4, are studied and discussed.

2. Results and discussion

The present MEDT study has been organized into six sections: i) the first section contains a topological analysis of the ELF at the ground state (GS) electronic structure of the reagents; ii) in the second section, an analysis of the reactivity indices at the GS of the reagents is conducted; iii) the third section explores the HB-catalysed P-DA reactions of Cp **4** with acrolein **5**; iv) the fourth section is focused on a comprehensive discussion of the origin of the *endo* selectivity in these HB-catalysed P-DA reactions; v) the fifth section presents a topological analysis of the electronic structure of the *endo* TSs based on ELF and the QTAIM; and finally, vi) the sixth section provides an IQA energy partitioning scheme and a REG analysis to determine the role of HB formation in improving the reaction rate.

2.1. ELF and QTAIM analysis of the electronic structure of the reagents

The topological analysis of the ELF [27] permits a quantitative characterisation of the electron density distribution in a molecule [37], allowing the establishment of a correlation between its electronic structure and its reactivity. Thus, an ELF topological analysis of the electronic structures of acrolein **5** and the HBMCs **6**, **18**, **24** and **26**, was performed first. ELF basin attractor positions, together with the most relevant valence basin populations, are shown in Fig. 2.

ELF topological analysis of acrolein **5** shows the presence of two disynaptic basins, V(C5,C6) and V' (C5,C6), integrating a total of 3.33 e, one V(C6,C7) disynaptic basin integrating 2.22 e, one V(C7,O8) disynaptic basin integrating 2.39 e, and two monosynaptic basins, V(O8) and V' (O8), integrating a total of 5.16 e (see Scheme 4 for atom numbering). While the population of the V(C7,O8) disynaptic basin allows relating the C7–O8 bonding region to a single bond, that of the V (C5,C6) and V' (C5,C6) disynaptic basins allows associating the C5–C6 bonding region with a depopulated double bond within Lewis's electronic structure model. The two V(O8) and V' (O8) monosynaptic basins are associated with non-bonding electron density regions at the O8 oxygen.

Formation of one HB between acrolein **5** and H_2O or $HCCl_3$, or two HBs with urea **16** or squaramide **25**, does not cause any remarkable changes in the ELF topology of the corresponding HBMCs with respect to that of acrolein **5** (see Fig. 2). A similar behaviour was found in the LA-catalysed reactions of acrolein **5** [13].

A natural population analysis [38,39] (NPA) of the atomic charges of acrolein **5** and HBMCs **6**, **18**, **24** and **26** was then carried out (see Fig. 2). As expected, the carbonyl C7 carbon of acrolein **5** presents a high positive charge, +0.41 e, while the O8 oxygen presents a high negative charge, −0.51 e, as a consequence of the strong polarization of the carbonyl C7–O8 bonding region. On the other hand, the β-conjugated C5 carbon of acrolein **5** presents a high negative charge, −0.29 e, owing to the more electronegative character of the C5 carbon compared to the two contiguous hydrogens.

Formation of one or two HBs of acrolein **5** with H_2O, $HCCl_3$, urea **16**, and squaramide **25** does not considerably change the natural atomic charges of the corresponding HBMCs compared to those of acrolein **5** (see Fig. 2). The only noticeable change is a slight increase in the polarization of the C7–O8 bonding regions towards the hydrogen-bonded carbonyl O8 oxygen.

Based on these ELF topological and NPA analyses at the GS of the reagents, it is possible to conclude that the formation of one or two HBs between acrolein **5** and the HB donors H_2O, $HCCl_3$, urea **16** or squaramide **25** does not significantly modify the electronic structure of this α,β-unsaturated carbonyl compound at its GS.

Finally, QTAIM [29,30] topological analysis of the electron density ρ at HBMCs **6**, **18**, **24**, and **26** was performed to characterize the O–H HB interactions at these species. The contour line maps of the Laplacian $\nabla^2\rho(r)$ of the electron density are shown in Fig. 3, while the calculated QTAIM parameters of the (3,-1) bonding critical points (CPs) characterising the HBs are given in Table S5 in Supplementary Material. At the four HBMCs, **CP1** and **CP2** show a positive Laplacian $\nabla^2\rho(r)$ value, indicating the absence of any covalent interaction (see Table S5 in Supplementary Material). At these HBMCs, the electron density at the two CPs is lower than 0.023. The electron density at the CPs in **6** and **18** is lower than that in **24** and **26**, respectively, indicating that the HB interactions in **24** and **26** are stronger than those at **6** and **18**.

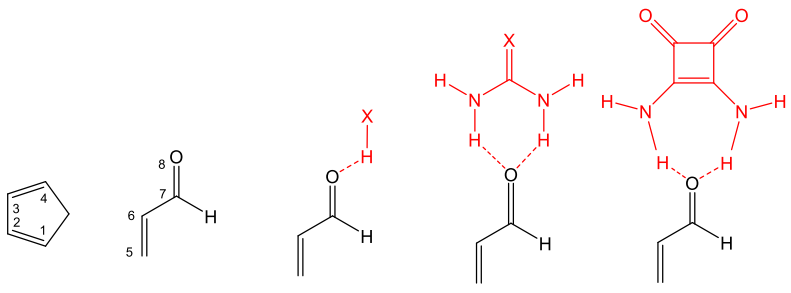

Scheme 4. Reagents involved in the non-catalysed and HB-catalysed P-DA reactions of Cp **4** with acrolein **5** studied herein.

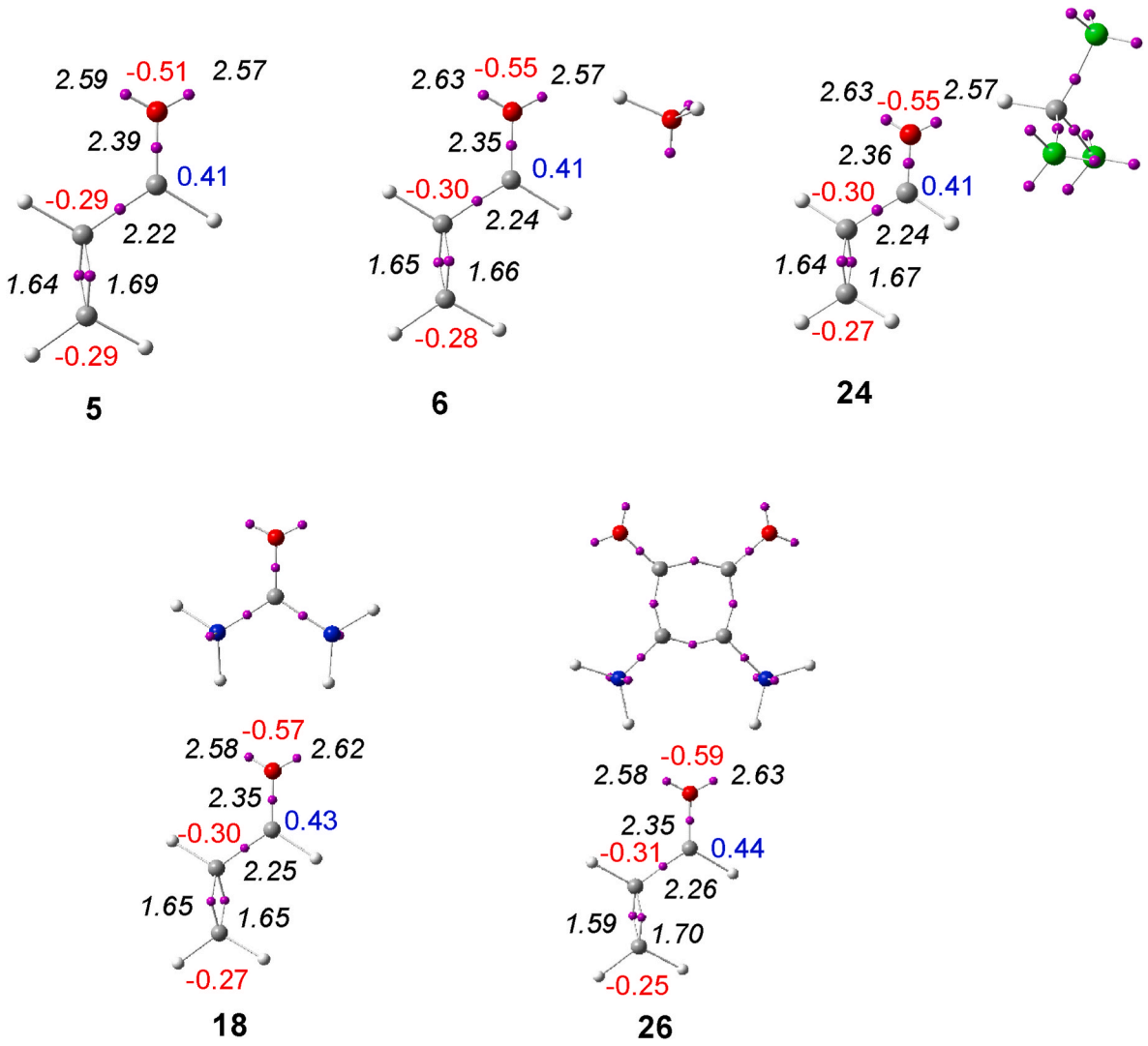

Fig. 2. ωB97X-D/6-311G(d,p) ELF basin attractor positions, populations of the most relevant valence basins, and natural atomic charges of acrolein **5** and the HBMCs **6**, **18**, **24** and **26**. Valence basin populations and natural atomic charges are given in average number of electrons, e. Valence basin populations are given in italics. Negative charges are coloured in red, and positive charges in blue.

Espinosa [40] proposed a useful criterion to characterize interactions at the CPs using an analysis of the ratio of the potential and kinetic energy electron density $|V(r)|/G(r)$. For ionic, non-covalent, and HB interactions, $|V(r)|/G(r) < 1$. Non-covalent interactions with somewhat covalent characters are characterised by $1 < |V(r)|/G(r) < 2$, while covalent interactions show $|V(r)|/G(r) > 2$. The calculated values of $|V(r)|/G(r)$ at the selected CPs in HBMCs **6**, **22**, **24**, and **26** are given in Table S5 in Supplementary Material. The $|V(r)|/G(r)$ values of **CP1** and **CP2** are lower than 0.91, indicating they are associated with HB interactions.

2.2. Analysis of the reactivity indices at the GS of the reagents

Many studies of P-DA reactions have shown that the reactivity indices [11,26] are powerful tools for understanding the reactivity in polar reactions [12]. The reactivity indices were calculated at the B3LYP/6-31G(d) computational level, which was employed to establish the electrophilicity and nucleophilicity scales [11]. The global reactivity indices, namely, the electronic chemical potential μ, chemical hardness η, global electrophilicity ω, and global nucleophilicity N, for Cp **4**, acrolein **5**, and the HBMCs **6**, **18**, **19**, **22**–**24**, **26** are given in Table 1.

The electronic chemical potential [41] μ of Cp **4**, $\mu = -3.01$ eV, is higher than that of acrolein **5**, $\mu = -4.38$ eV, and those of the corresponding HBMCs, $\mu > -3.82$ eV (Acr:thiourea **19**) (see Table 1), indicating that the GEDT will take place from Cp **4** towards these ethylene derivatives. Thus, these P-DA reactions will be classified as a forward electron density flux (FEDF) [42,43].

According to the electrophilicity ω and nucleophilicity N indices, Cp **4** is classified on the borderline of moderate electrophiles, $\omega = 0.83$ eV, and as strong nucleophile, $N = 3.36$ eV, thus participating in P-DA reactions as a strong nucleophile without requiring nucleophilic activation.

Acrolein **5** is classified as a strong electrophile, $\omega = 1.84$ eV, and as moderate nucleophile, $N = 2.12$ eV. Formation of the HBs with the carbonyl oxygen of acrolein **5** causes a remarkable increase of the electrophilicity ω index of these HBMC species as they are all higher than 2.09 eV (see Table 1). Within the series of ROH, the electrophilicity ω index of the corresponding HBMC increases in the order 2.09 (**22**, R = Me) < 2.10 (**6**, R=H) < 2.56 (**23**, R=CF_3) eV, as a consequence of an increase of the acid character of the alcohol hydrogen. Notably, the electrophilicity ω index of the non-classical HBMC **24** (Acr:$HCCl_3$), $\omega = 2.25$ eV, is higher than those of HBMCs **6** (Acr:H_2O) and **22** (Acr:CH_3OH). As expected, the bifunctional HBMC **18** (Acr:urea), **19** (Acr:thiourea) and **26** (Acr:squaramide) present the highest electrophilicity ω

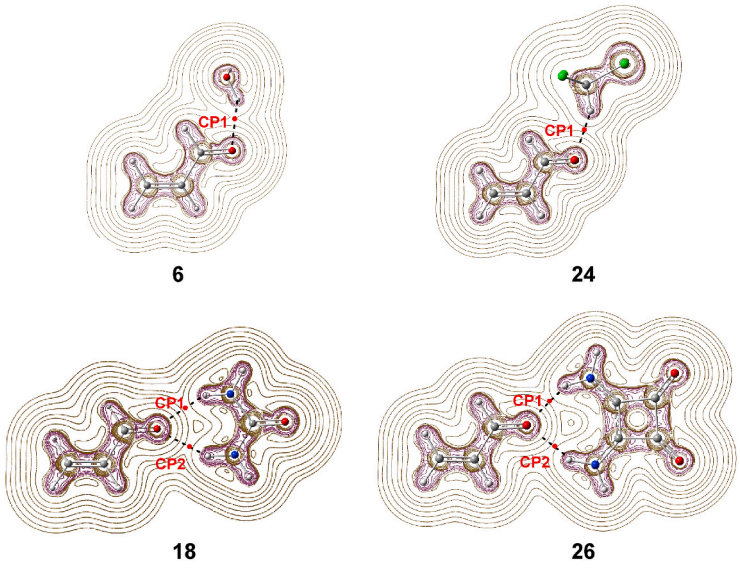

Fig. 3. Representations of the contour line maps of the Laplacian $\nabla^2\rho$(r)of the electron density at HBMCs **6**, **18**, **24**, and **26**. The critical points **CP1** and **CP2** are coloured in red.

Table 1
B3LYP/6-31G(d) electronic chemical potential μ, chemical hardness η, electrophilicity ω, and nucleophilicity *N*, in eV, for Cp **4**, acrolein **5** and the HBMCs **6**, **18**, **19**, **22**–**24**, **26**.

Compound	μ	η	ω	*N*
Acr:squaramide **26**	−4.00	2.10	3.81	4.07
Acr:thiourea **19**	−3.82	2.09	3.49	4.26
Acr:urea **18**	−4.31	3.60	2.58	3.01
Acr:CF_3OH **23**	−5.31	5.51	2.56	1.05
Acr:$HCCl_3$ **24**	−4.90	5.34	2.25	1.56
Acr:H_2O **6**	−4.71	5.28	2.10	1.77
Acr:MeOH **22**	−4.42	4.67	2.09	2.37
acrolein **5**	−4.38	5.23	1.84	2.12
Cp **4**	−3.01	5.49	0.83	3.36

values, 2.58, 3.49, and 3.81 eV, respectively. It is expected that squaramide **25** will be the most efficient hydrogen donor of this series. Consequently, the DA reactions of Cp **4**, a strong nucleophile, with these HBMCs, classified as strong electrophiles, are expected to exhibit a high polar character [8].

The analysis of Parr functions [44] allows to characterize the most electrophilic and nucleophilic centres of a molecule involved in the P-DA reaction, allowing to characterize the more factorable two-centre interactions at the polar TSs [12]. The electrophilic P_k^+ Parr functions of acrolein **5** and its HBMCs **18**, **24** and **26** are given in Fig. 4.

Analysis of the electrophilic P_k^+ Parr functions of acrolein **5** indicates that the β-conjugated C5 carbon is the most electrophilic centre of this α,β-unsaturated aldehyde, $P_k^+ = 0.52$. In fact, this position is twice as electrophilically activated as the carbonyl C7 carbon, $P_k^+ = 0.25$. Formation of one or two HBs with the carbonyl O8 oxygen of acrolein **9** slightly increases the electrophilic P_k^+ Parr functions at the carbonyl C7 carbon of HBMCs **18**, **24**, and **26**. Still, the β-conjugated C5 carbon remains the most electrophilic centre of these HBMCs.

A slight decrease of the electrophilic P_k^+ Parr functions is observed at HBMC **24** (Acr:$HCCl_3$), as a consequence of the electrophilic activation

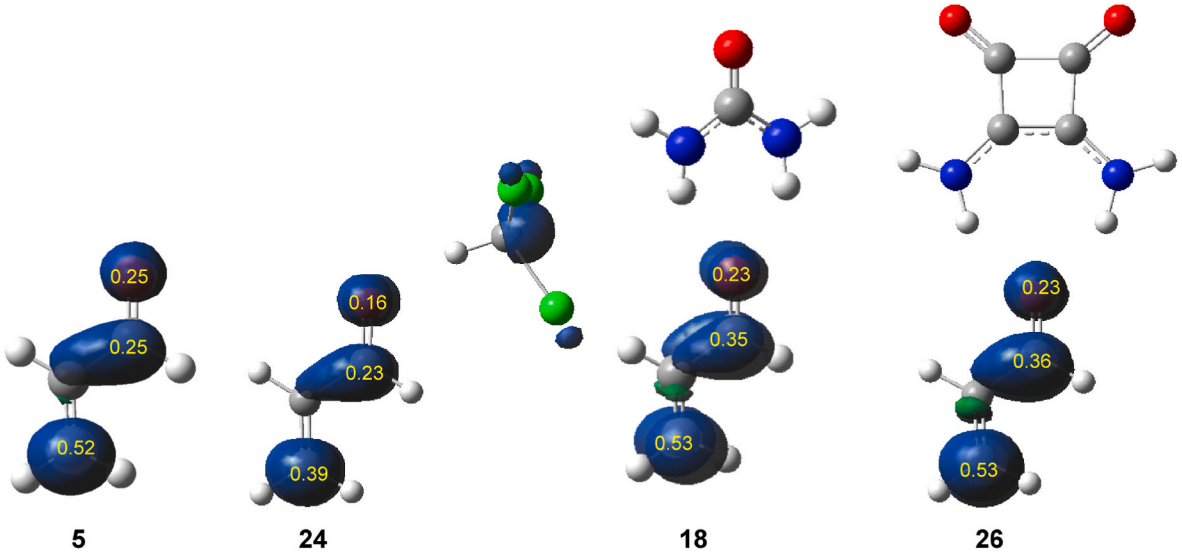

Fig. 4. 3D representations of the Mulliken atomic spin densities of the radical anion of acrolein **5**$^{\cdot-}$ and those of HBMCs **18**$^{\cdot-}$, **24**$^{\cdot-}$ and **26**$^{\cdot-}$, together with the electrophilic P_k^+ Parr functions of acrolein **5** and HBMCs **18**, **24** and **26**.

of the carbon atom of $HCCl_3$, but it does not change the electrophilic relationship between the C5 and C7 carbons of acrolein **5**. Consequently, along a P-DA reaction involving these non-symmetric electrophilic species, the asynchronicity in the C–C single bond formation will be determined by the preferential C–C bond formation at the most electrophilic C5 carbon of these HBMC species [45].

It is worth emphasizing that the C5 carbon of these α,β-unsaturated carbonyl compounds, which is the most electrophilic centre of these species, is negatively charged by more than −0.25 e (see Fig. 2). This finding supports Domingo's proposal made in 2012, which suggested that the local electrophilic/nucleophilic behaviours of organic molecules are not simply caused by charges [45]. The most electrophilic centre of a molecule is the one that accepts the highest amount of electron density resulting from the nucleophilic/electrophilic interactions taking place along the approach of the two reagents. Interestingly, in some cases, such as in acrolein **5**, the most electrophilic β-conjugated C5 carbon is negatively charged, while the most positively charged C7 carbon, +0.41 e, is only half as electrophilically activated as the C5 carbon [13].

2.3. Study of the HB-catalysed P-DA reactions of acrolein *5* with Cp *4*

To shed light on the role of the HB formation on the P-DA reactions of Cp **4** with HBMCs **6**, **18**, **19**, **22**–**24** and **26**, the DA reaction of Cp **4** with acrolein **5** was first studied as the energy reference for the non-catalysed process; the corresponding study is given in Section 2 of Supplementary Material. Due to the non-symmetry of the electrophilic C5–C6 ethylene of acrolein **5**, two stereoisomeric reaction paths, the *endo,* and the *exo*, are feasible in these HB-catalysed P-DA reactions (Scheme 5). The search for stationary points involved in these P-DA reactions allowed locating two stereoisomeric transition state structures (TSs), **TSn-X** and **TSx-X**, and the corresponding cycloadducts (CAs), **CAn-X** and **CAx-X**, indicating that they take place through a one-step mechanism (Scheme 5). Gas phase relative electronic energies are given in Table 2, while total energies are gathered in Table S6 in Supplementary Material.

Full optimization of the stationary points associated with the P-DA reactions involving bifunctionalised urea **16**, thiourea **17**, and squaramide **25** as HB catalysts gives a series of TSs in which the catalyst framework is positioned near the Cp one. This behaviour is due to favourable NCI [31] taking place between the nitrogens these catalysts and some hydrogen atoms of Cp **5**. A complete analysis of the corresponding P-DA reactions is given in Section 3 in Supplementary Material. Given the significance of these NCI, which can be stronger than the HB catalytic effects of these species, the dihedral angles defining the nitrogen atoms linked to the acidic hydrogens of these catalysts were frozen to the values at the GS of HBMCs **18**, **19** and **26**; i.e. N–H–*O*–C

Table 2
ωB97X-D/6-311G(d,p) gas phase relative energies, in kcal·mol^{-1}, of the stationary points involved in the P-DA reactions between Cp **4** and HBMCs **6**, **18**, **19**, **22**–**24** and **26**.

X =	**22**	**6**	**24**	**23**	**18**	**19**	**26**
TSn-X	11.8	11.9	11.3	10.7	10.8	10.2	9.6
TSx-X	12.3	12.4	12.0	11.3	11.3	10.7	10.2
CAn-X	−29.4	−29.3	−29.6	−29.3	−29.2	−29.6	−29.8
CAx-X	−29.1	−29.0	−29.2	−28.9	−29.1	−29.2	−29.3

dihedral angles were fixed to 180°. These geometrical constraints are commonly employed in the theoretical study of enzymatic reactions, where the positions of the amino acids are frozen to those in the natural enzyme [46,47]. On the other hand, within the reaction medium, the reagents are surroundings of solvent molecules, rendering the intramolecular NCI present in the fully optimized TSs potentially irrelevant. Thus, when two solvent water molecules are implicitly included in the calculations, the aforementioned fully optimized TSs do not exist (see Section 3 in Supplementary Material).

The activation energies associated with these HB-catalysed DA reactions range from 11.9 (**TSx-6**) to 9.6 (**TSn-26**) kcal mol^{-1}. The reactions are exothermic by more than 29 kcal mol^{-1}. Some appealing conclusions can be obtained from the relative energies given in Table 2: i) the HB-catalysed DA reactions of Cp **4** with acrolein **5** are between 1.7 (**TSn-6**) and 4.0 (**TSn-26**) kcal mol^{-1} lower in energy than that of the non-catalysed DA reaction (see Section 2 in Supplementary Material for the activation energy of the non-catalysed process), indicating a moderate catalytic effect of the formation of HBs with acrolein **5**; ii) the activation energy of the DA reaction of Cp **4** with HBMC **23** (Acr:CF_3OH) having one HB, 10.7 kcal mol^{-1} (**TSn-23**), is closer to that with HBMC **18** (Acr:urea) having two HB, 10.8 kcal mol^{-1} (**TSn-18**), in agreement with the similar electrophilic character of HBMCs **23** and **18** (see Table 1); iii) the highest catalytic effect is found in the P-DA reactions involving bifunctionalised squaramide **25**, 9.6 kcal mol^{-1} (**TSn-26**), in agreement with the highest electrophilicity ω index of HBMC **26** (Acr:squaramide) (see Table 1); iv) these HB-catalysed DA reactions are low *endo* stereoselective as the *endo* **TSn-X** are by only 0.5–0.7 kcal mol^{-1} below the *exo* **TSx-X**; v) the *endo* stereoselectivity found in all of these HB-catalysed DA reactions, which is similar to that found in LA-catalysed DA reactions [13], are in agreement with the *endo* stereoselectivity found experimentally in the HB-catalysed DA reactions of bifunctionalised thioureas (see later [48,49]); and finally, vi) the exothermic character of these HB-catalysed DA reactions, between −29.0 and −29.9 kcal mol^{-1}, is close to that of the non-catalysed DA reaction, −29.0 kcal mol^{-1} (see Section 2 of Supplementary Material). These high values render these DA reactions irreversible and thus under

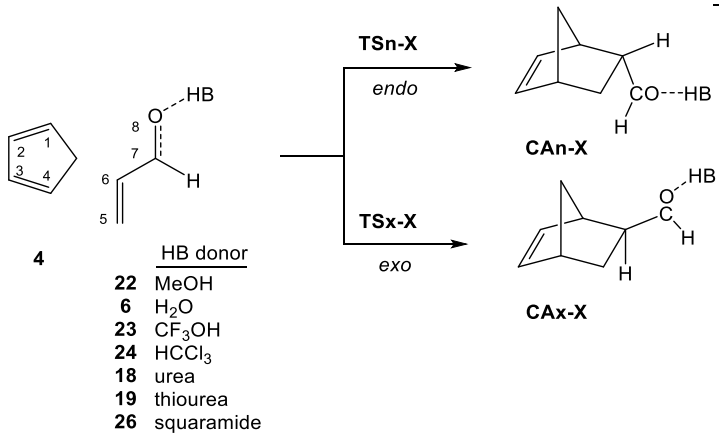

Scheme 5. P-DA reactions of Cp **4** with HBMCs **6**, **18**, **19**, **22**–**24**, **26**.

kinetic control.

Due to the polar character of the TSs involved in these HB-catalysed DA reactions, solvent effects of water were considered in the squaramide HB-catalysed DA reaction of Cp **4** with acrolein **5**. Table S7 in Supplementary Material gives the total and relative energies. Solvent effects decrease the activation energy of the non-catalysed DA reaction of Cp **4** with acrolein **5** by 0.7 kcal mol^{-1}, while the low *endo* stereoselectivity found in the gas phase is not modified in water. Unexpectedly, the activation energy of the most favourable *endo* reaction path of the DA reaction of Cp **4** with HBMC **26** (Acr:squaramide) in water experiences a slight increase of 0.3 kcal mol^{-1} with respect to the gas phase reaction as a consequence of slightly better solvation of HBMC **26** than **TSn-26**. In water, the squaramide HB-catalysed DA reaction remains somewhat *endo* stereoselective. Consequently, solvent effects, as calculated within the PCM approximation, do not cause any remarkable change in these HB-catalysed DA reactions.

The geometries of some representative *endo* TSs associated with the HB-catalysed DA reactions of Cp **4** with acrolein **5** are given in Fig. 5, while the most relevant parameters and geometrical asynchronicities $\Delta l = d(C1–C6) - d(C4–C5)$ of all TSs are given in Table 3. As can be observed, there is a great similitude in the geometries of the four TSs given in Fig. 5. While the distances between the C4 and C5 interacting carbons are found in the short range of 2.04–2.06 Å, those between the C1 and C6 carbons are between 2.42 and 2.48 Å (see Table 3). These distances indicate that these TSs are associated with asynchronous C–C single bond formation processes, resulting from the nucleophilic attack of the C4 carbon of Cp **4** on the most electrophilic centre of these α,β-unsaturated carbonyl compounds, the β-conjugated C5 carbon, in agreement with the analysis of the electrophilic Parr functions of these HBMCs (see Fig. 4). As the C–C single bond formation in cycloaddition reactions takes place in the short range of 1.9–2.0 Å [7], these distances indicate that the formation of either C–C single bond has not yet begun at any TS (see later).

Due to the more polar character of the HB-catalysed TSs than the non-catalysed ones, the former is more asynchronous, $\Delta l > 0.36$ than the latter, $\Delta l = 0.28$ (see Table 3 and Fig. S1 in Supplementary Material). The decrease in the activation energy with HB formation is accompanied by a slight increase of the geometrical asynchronicity Δl, which ranges from 0.26 to 0.48 (see Table 3). In addition, the less favourable *exo* TSs are slightly more asynchronous than the *endo* ones.

Table 3
Selected geometrical parameters, in angstroms, Å, of the TSs associated with the HB-catalysed DA reactions between Cp **4** and acrolein **5**, Δl represents the geometrical asynchronicity. GEDT values computed at the TSs are given in average number of electrons, e.

	C4–C5	C1–C6	O8–H	O8–H′	Δl	GEDT
TSn-6	2.061	2.423	1.916		0.36	0.17
TSx-6	2.061	2.448	1.919		0.39	0.18
TSn-22	2.060	2.427	1.882		0.37	0.18
TSx-22	2.060	2.452	1.885		0.39	0.18
TSn-23	2.042	2.475	1.621		0.43	0.21
TSx-23	2.043	2.503	1.626		0.46	0.21
TSn-24	2.056	2.433	1.996		0.38	0.18
TSx-24	2.055	2.459	2.005		0.40	0.18
TSn-18	2.050	2.451	2.057	2.105	0.40	0.19
TSx-18	2.049	2.482	2.057	2.108	0.43	0.20
TSn-19	2.043	2.471	2.021	2.046	0.43	0.21
TSx-19	2.042	2.503	2.021	2.048	0.46	0.21
TSn-26	2.039	2.480	2.005	2.021	0.44	0.22
TSx-26	2.038	2.514	2.008	2.020	0.48	0.22

The HB H–O distances at the TSs are slightly smaller than those at the corresponding HBMCs due to the increase of the non-bonding electron density of the carbonyl O8 oxygen at the polar TSs (see Fig. S8 in Supplementary Material).

Analysis of the GEDT at the TSs involved in these HB-catalysed DA reactions permits quantifying the polar character of these DA reactions [7,8]. Table 3 includes the GEDT values computed at all TSs. GEDT values lower than 0.05 e correspond to non-polar processes, while values higher than 0.20 e correspond to highly polar processes. The GEDT value of the non-catalysed DA reaction is 0.14 e (**TSn-5**), indicating that this DA reaction has some polar character (see Section 2 in Supplementary Material). Higher GEDT values are found at the TSs involved in the HB-catalysed DA reactions, which range from 0.17 to 0.22 e, indicating that the corresponding DA reactions have a more polar character. The GEDT values at the TSs involving squaramide **25** are slightly higher than those involving urea **16** and thiourea **17**, a trend anticipated by analysis of the electrophilicity ω indices of the corresponding HBMCs **18**, **19**, and

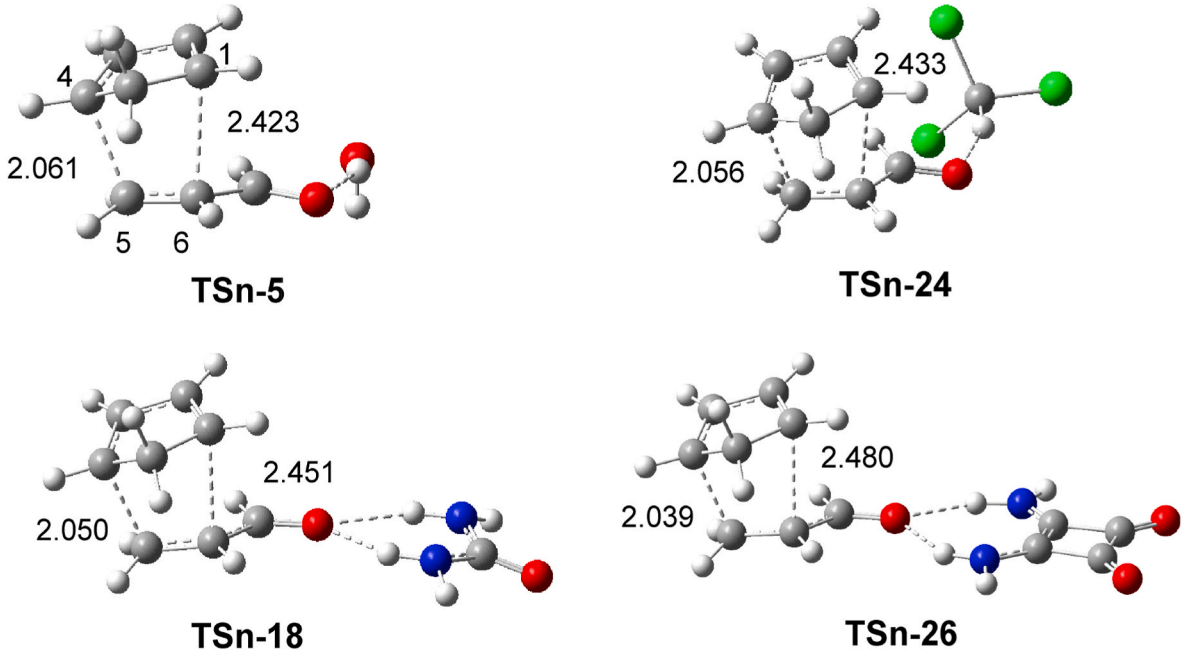

Fig. 5. ωB97X-D/6-311G(d,p) optimized geometries of some *endo* TSs associated with the HB-catalysed DA reactions of acrolein **5** with Cp **4**. Distances between the interacting carbons are given in angstroms, Å.

26 (see Table 1).

To understand the role of the GEDT taking place at the *endo* and *exo* TSs in the decrease of the activation energies ΔE_{act} of these HB-catalysed DA reactions, a representation of ΔE_{act} vs. the GEDT at the TSs was performed (see Fig. 6). The GEDT values at the non-catalysed, 0.14 e at **TSn-5 and TSx-5,** and the BH_3 LA-catalysed DA reaction, 0.27 (*endo* TS) and 0.26 (*exo* TS) e [13], are also included. As can be observed, a very good linear correlation between the gas phase ΔE_{act} and the GEDT computed at the twelve TSs is found, $R^2 = 0.94$ (see Fig. 6). This trend is similar to that observed in the study of P-DA reactions [8] (see Fig. 1) and in the study of LA-catalysed DA reactions [13].

Fig. 6 shows that the low polar DA of Cp **4** with acrolein **5** is located in the upper left-hand side of the linear correlation, while the high polar LA catalysed DA reaction involving the BH_3:acrolein complex **7** [13] (see Fig. 2) is located in the bottom right-hand side position. Deviation of the linearity is due to other favourable/unfavorable stereoelectronic interactions at specific TSs.

When the *endo* and *exo* fully optimized TSs involving urea **16**, thiourea **17**, and squaramide **25** are included in Fig. 6, the coefficient of determination R^2 of the linear regression decreases to 0.74 (see the pink dots in Fig. 6). This behaviour indicates that these TSs do not fit the relationship between the decrease in activation energy and the increase in GEDT, which reflects the polar character of the HB-catalysed DA reactions (see also Fig. 1). Note that the activation energies of the fully optimized TSs are even lower than those in the LA BH_3-catalysed reaction (as shown by the blue dots in Fig. 6).

Three regions can be clearly differentiated in Fig. 6: i) the non-catalysed DA reaction between Cp **4** and acrolein **5** with $\Delta E_{act} > 13$ kcal mol^{-1} and GEDT <0.15 e; ii) HB-catalysed DA reactions involving HBMCs **6**, **18**, **19**, **22**–**24**, **26** with $13 < \Delta E_{act} < 9$ kcal mol^{-1} and 0.15 < GEDT <0.25 e; and finally iii) the BH_3 LA-catalysed DA reaction with $\Delta E_{act} < 8$ kcal mol^{-1} and GEDT >0.25 e. As can be seen in Fig. 6, the HB-catalysed DA reactions involving urea **16**, thiourea **17**, and squaramide **25** are found in the bottom right-hand side position of the HB-catalysed DA reaction series. These findings, which have been found in numerous polar cycloaddition reactions [8,13], support the proposal that the GEDT taking place in P-DA reactions plays a significant role in the decrease of the activation energies of the reactions (see section 2.6) [8,50].

Finally, the graphical representation in Fig. 7 illustrates a strong linear correlation between the geometrical asynchronicity (Δl) at the *endo*, $R^2 = 0.98$, and *exo*, $R^2 = 0.99$, TSs and the GEDT. This analysis suggests that in P-DA reactions involving non-symmetric electrophilic ethylenes, the higher the GEDT, the more asynchronous the DA reaction [10]. This behaviour arises due to the strengthening of the two-centre nucleophilic/electrophilic interactions between C4 and C5 carbons at the polar TSs, while the interaction between the non-interacting centres C1 and C6 decreases, explaining the decrease in the so-called Pauli repulsion resulting from closed-shell intermolecular repulsions between non-bonded molecules [51] (see the Δl the TSs in Table 3).

2.4. What is the origin of the endo selectivity in these HB-catalysed P-DA reactions?

In 2003, Schreiner et al. [48,49] experimentally studied the catalytic activity of substituted aryl thioureas such as **27** in a series of DA reactions (see Scheme 6). They found that the effect of HBs were similar to those observed with mild LAs. Formation of the two HBs of thiourea **27** to the carbonyl oxygen of crotonaldehyde **28** slightly increases the *endo* selectivity in the corresponding DA reaction with respect to the reaction without catalyst (see Scheme 6).

Endo stereoselectivity is explained within the FMO theory [23] by secondary orbital interactions (SOI) present at the *endo* TSs, a concept introduced in 1983 by Gleiter and Bohm to explain the regio- and stereoselectivity in DA reactions [52].

In 1999, Domingo proposed that the *endo* stereoselectivity in P-DA reactions results from the favourable electrostatic interactions existing in the *endo* zwitterionic TSs [53]. In 2000, Salvatella et al. proposed that a combination of well-known mechanisms, such as solvent effects, steric interactions, HBs, electrostatic forces, and others, can be invoked

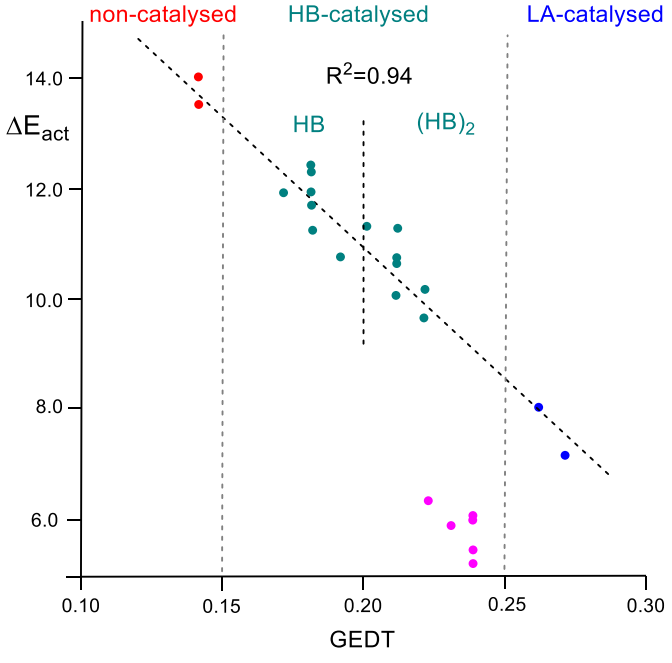

Fig. 6. Plot of the activation energies, ΔE_{act}, in kcal·mol^{-1}, of the HB-catalysed DA reactions of acrolein **5** with Cp **4**, in green, vs the GEDT, in average number of electrons e, computed at the corresponding *endo* and *exo* TSs. The non-catalysed, in red, and the LA BH_3-catalysed DA reactions, in blue, are also included. Activation energies of the fully optimized TSs involving HBMCs **18**, **19** and **26** are represented by pink dots.

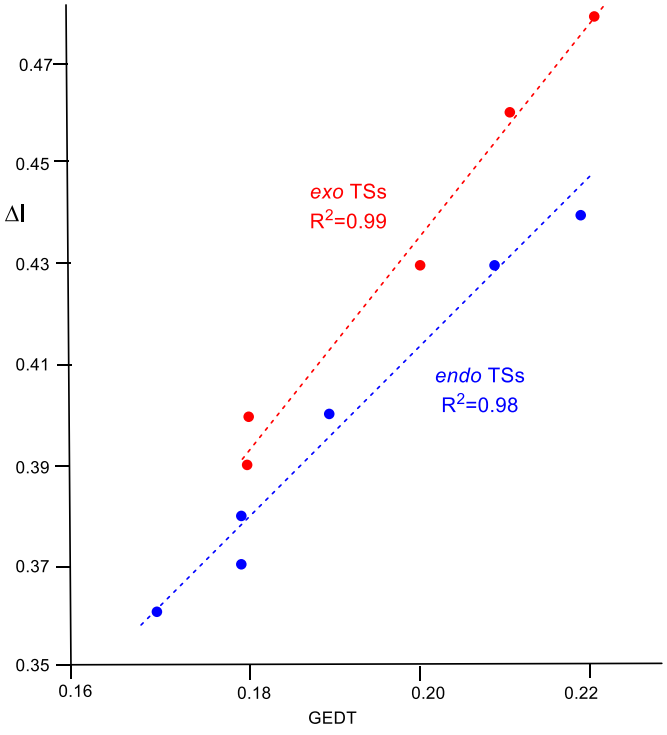

Fig. 7. Plot of the geometrical asynchronicity, Δl, in angstroms, Å, at the *endo* TSs, in blue, and the *exo* TSs, in red, associated with the HB-catalysed DA reactions of Cp **4** with acrolein **5**, vs. the GEDT, in average number of electrons, e.

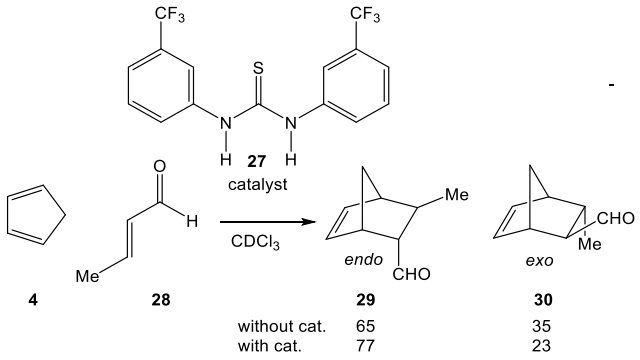

Scheme 6. BH-catalysed DA reaction of Cp **4** with crotonaldehyde **28**.

instead of SOI in the *endo/exo* selectivity of DA reactions [54]. Note that $\Delta\Delta TS_{endo\text{-}exo}$ is less than 0.7 kcal mol^{-1} in these HB-catalysed DA reactions. Consequently, it is difficult to attribute a single factor responsible for the *endo/exo* stereoselectivity.

An analysis of the geometries of **TSn-19** and **TSx-19** associated with the thiourea-catalysed DA reaction of Cp **4** with acrolein **5** allows obtaining some appealing conclusions (see the geometries of the two TSs in Fig. S9 in Supplementary Material): i) the main geometric difference between the two stereoisomeric TSs is the relative position of the carbonyl C=O group with respect to the unsaturated framework of Cp. At the more favourable *endo* **TSn-19**, the carbonyl C=O group is positioned above the unsaturated framework of Cp, while at the *exo* **TSx-19**, it is farther away; ii) the GEDT taking place at these polar TSs causes that while the carbonyl CO group increases its negative charge, the unsaturated framework of nucleophilic Cp becomes positively charged. Consequently, it is expected that the favourable attractive electrostatic interactions present at the *endo* **TSn-19** cause a slight decrease in the distance between the two non-interacting C1 and C6 carbons, thus decreasing the asynchronicity Δl at the *endo* TSs (see Fig. S9 in Supplementary Material and the asynchronicity Δl in the all *endo/exo* TSs in Table 3). Note that the C4–C5 distances are practically unchanged at the pairs of the *endo/exo* TSs. Similar behaviours are found in the *endo* TSs associated with P-DA reactions [13] and LA-catalysed DA reactions [53].

2.5. ELF and QTAIM topological analysis of the electronic structure of the endo TSs involved P-DA reactions of Cp *4* with acrolein *5* and the series of HBMCs *6*, *18*, *24*, and *26*

A comparative ELF topological analysis of the *endo* TSs **TSn-5**, **TSn-6**, **TSn-18**, **TSn-24** and **TSn-26** was performed to understand how HB formation modifies the molecular mechanism of these HB-catalysed DA relations. The ELF basin attractor positions are shown in Fig. 8, while the populations of the more relevant valence basins are given in Table 4.

As can be seen, the four catalysed TSs present the same ELF topology as the non-catalysed **TSn-5**, indicating that they have a similar electronic structure to that associated with the non-catalysed DA reaction between Cp **4** and acrolein **5**. The most relevant feature of the five TSs is the presence of two V(C4) and V(C5) monosynaptic basins, integrating ca. 0.32 and 0.24 e, respectively, at the two C4 and C5 interacting carbons. Note that these monosynaptic basins, which are not present at the reagents (see Fig. 2), characterize the C4 and C5 carbons as two *pseudoradical* centres [55], which are demanded for the formation of the first C4–C5 single bond in a subsequent stage of the reaction [7]. On the other hand, the C1–C2, C3–C4 and C5–C6 bonding regions of the Cp and acrolein frameworks at the five TSs, which were characterized by the presence of two disynaptic basins, V(Ci,Cj) and V' (Ci,Cj) at the GS of the reagents (see Fig. 2), are characterized by the presence of only one V(Ci, Cj) disynaptic basin, integrating ca. 2.7 e (V(C1,C2)), 2.9 e (V(C3,C4)) and 2.9 e (V(C5,C6)). These topological changes result from the depopulation of the C1–C2, C3–C4, and C5–C6 bonding regions, a behaviour demanded to create the new V(C4) and V(C5) monosynaptic basins. The presence of neither V(C4,C5) nor V(C1,C6) disynaptic basins indicates that the formation of the new C4–C5 and C1–C6 single bonds has not started at any TS yet, as was commented on in the previous analysis of the TSs geometries.

Finally, the nature of the C4–C5, C1–C6, and O8–H electronic interactions at **TSn-6**, **TSn-18** and **TSn-24**, associated with a classical, non-classical, and double HB-catalysed DA reactions, was studied by an QTAIM topological analysis of the electron density ρ at the (3,-1) bonding CPs. The contour line maps of the Laplacian $\nabla^2\rho(r)$ of the electron density are shown in Fig. 9, while the calculated QTAIM

Table 4
Population of the most relevant valence basins at **TSn-5, TSn-6, TSn-18, TSn-24** and **TSn-26**. Valence basin populations are given in an average number of electrons, e.

	TSn-5	TSn-6	TSn-24	TSn-18	TSn-26
V(C1,C2)	2.71	2.67	2.67	2.66	2.65
V(C2,C3)	2.72	2.70	2.71	2.70	2.69
V(C3,C4)	2.95	2.94	2.94	2.93	2.93
V(C5,C6)	2.95	2.90	2.89	2.89	2.85
V(C4)	0.32	0.36	0.36	0.36	0.38
V(C5)	0.24	0.26	0.26	0.26	0.26

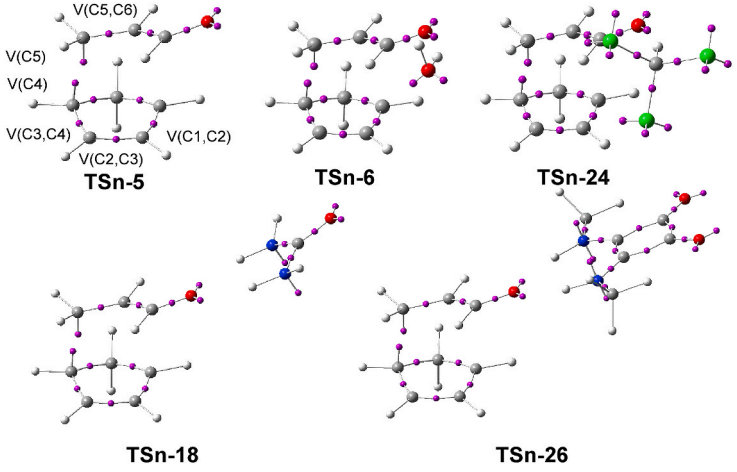

Fig. 8. ELF basin attractor positions, together with the most relevant valence basin populations, of the *endo* TSs involved in the P-DA reactions of Cp **4** with acrolein **5** and HBMCs **6**, **18**, **24**, and **26**.

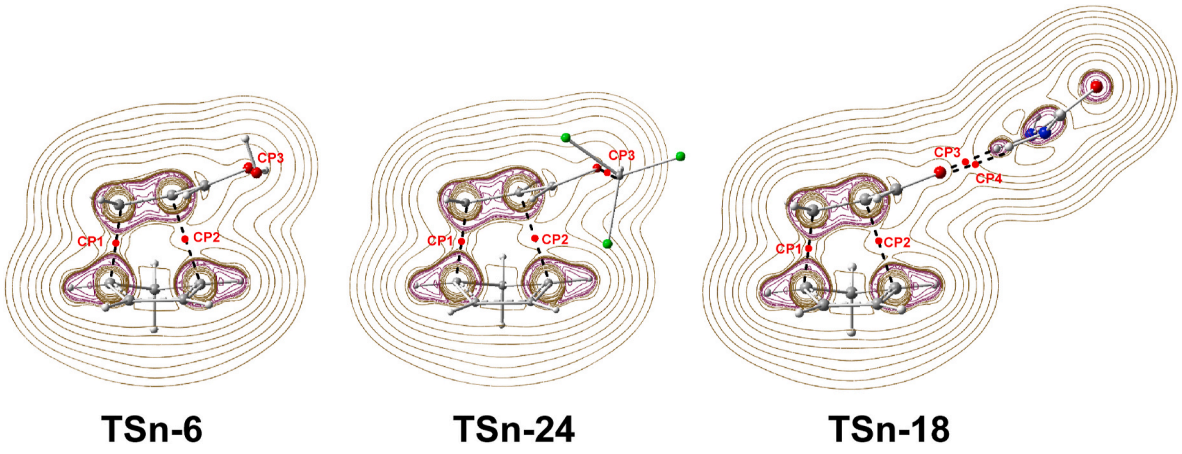

Fig. 9. Representations of the contour line maps of Laplacian $\nabla^2\rho(r)$ of the electron density at **TSn-6**, **TSn-18** and **TSn-24**. The bonding critical points **CPi** are labelled in red.

parameters are given in Table S8 in Supplementary Material.

At the three TSs, **CP1** and **CP2**, associated with the C4–C5 and C1–C6 interacting regions, respectively, present positive Laplacian $\nabla^2\rho(r)$ values, indicating the absence of any covalent interaction between the two pairs of interacting carbons (see Table S8 in Supplementary Material). On the other hand, at the three TSs, the electron density at **CP1**, ca. 0.076 e, is twice that at **CP2**, ca. 0.038 e, indicating a stronger electronic interaction at the C4–C5 region than at the C1–C6 one, in agreement with the analysis of the Parr functions. These results support the more favourable gathering of electron density at the most nucleophilic and electrophilic centres as a consequence of the GEDT taking place in polar reactions, which is responsible for the TSs asynchronicity. Finally, the slight decrease of the electron density $\rho(r)$ at **CP2**, which diminishes as the asynchronicity Δl increases at these TSs, accounts for the reduction in the proposed Pauli repulsions [17].

The calculated values of $|V(r)|/G(r)$ at the selected bonding CPs associated with the three TSs are given in Table S8 in Supplementary Material. According to Espinosa's criterion [40], the $|V(r)|/G(r)$ values at **CP1** and **CP2**, ca. 1.80 and 1.24, respectively, indicate that they are associated with non-covalent interactions with somewhat covalent character, while the $|V(r)|/G(r)$ values at **CP3** and **CP4**, related to the O8–H and O8–H′ bonding regions, respectively, are lower than 0.94, indicating that they are associated with HB interactions.

The present ELF and QTAIM topological analyses of the electron density of **TSn-6**, **TSn-18** and **TSn-24** show a complete similitude between the electronic structures of the three selected TSs, in total agreement with their similar geometries. These findings indicate that formation of the HBs with the carbonyl oxygen atom of acrolein **5** does not substantially modify the electronic behaviour of **TSn-5**, associated with the non-catalysed process, thus being the different GEDT values at the three TSs the only property that makes these species different.

Finally, a BET study of the molecular mechanisms of the non-catalysed DA reactions of Cp **4** with acrolein **5**, and that of the catalysed DA reaction with HBMC **18** shows the great similitudes between them. The mechanism of both DA reactions is divided in eleven *phases* characterizing these DA reactions as non-concerted *two-stage one-step* processes [56]. The complete BET analyses are given in Section 4 in Supplementary Material.

2.6. IQA and REG-IQA analyses of the role of HB formation in improving the reaction rate

First, the role of the increase in GEDT, resulting from the HB formation, in the decrease of activation energies in the P-DA reactions was studied by a topological IQA energy partitioning analysis using four selected TS of increasing polar character. These TSs are associated with the N-DA reaction of Cp **4** with ethylene **2**, which is taken as the energy reference, as well as those of the P-DA reaction of Cp **4** with acrolein **5**, and with complexes HBMC **23** and acrolein:LA **7** (see Figs. 1 and 6). The B3LYP/6-311G(d,p) gas-phase relative total $E_{tot}(X)$, intra-atomic $E_{intra}(X)$ and interatomic $V_{inter}(X)$ IQA energies of the Cp and ethylene (Et) interacting quantum fragments [57,58] (IQF) of the four TSs, with respect to those at the separated reagents, are given in Table 5 (see the Computational Details in Supplementary Material). Fig. 10 shows a graphical representation of the relative $E_{tot}(X)$ energies of the Cp and Et IQFs at the four TSs, in blue and red, respectively, and the relative $E_{tot}(Cp + Et)$ energies, in black, which corresponds to the activation energies of these DA reactions.

Analysis of the $E_{tot}(X)$ energies of the two IQFs in the N-DA reaction of Cp **4** with ethylene **2** shows that both IQFs are destabilized by ca. 11 kcal mol^{-1}. Interestingly, while the intra-atomic $E_{intra}(Cp + Et)$ energies in this N-DA reaction are very unfavorable, 72.0 kcal mol^{-1}, the interatomic $V_{inter}(Cp + Et)$ energies are very favourable by −49.3 kcal mol^{-1}.

An interesting change is observed in the P-DA reactions involving the three substituted ethylenes of increasing electrophilicity. While the unfavorable $E_{tot}(Cp)$ energies increase with the increase of the GEDT at the TS, i.e., the Cp IQF is destabilized due to the loss of electron density, those of the ethylene $E_{tot}(Et)$ become negative, and consequently, stabilizing, as a result of the gain of electron density (see Fig. 10). Interestingly, the stabilization of the ethylene IQF overcomes the Cp destabilization, thus resulting in a decrease of the activation energy with the increase of the polar character of the reaction (see Fig. 10).

A more detailed analysis of the $E_{intra}(Et)$ and $V_{inter}(Et)$ IQF energies given in Table 5 reveals that the decrease of the unfavorable $E_{intra}(Et)$ energies of the ethylene IQF with the increase of the GEDT taking place

Table 5
B3LYP/6-311G(d,p) gas-phase relative total $E_{tot}(X)$, intra-atomic $E_{intra}(X)$ and interatomic ($V_{inter}(X)$) IQA energies, in kcal·mol^{-1}, of the Cp and ethylene IQF at the TSs with respect to the separated reagents. Standard deviations are given with respect to the N-DA reaction of Cp **4** with ethylene **2**, in kcal·mol^{-1}.

	IQF	$E_{intra}(X)$	$V_{inter}(X)$	$E_{tot}(X)$	$E_{tot}(Cp + Et)$
Ethylene **2**	Cp	36.7	−25.2	11.5	22.7
	Et	35.3	−24.1	11.2	
Acrolein **5**	Cp	40.2	−17.5	22.7	19.2
	Et	25.3	−28.7	−3.4	
CHO–HOCF$_3$ **23**	Cp	41.0	−10.8	30.2	15.5
	Et	12.4	−27.1	−14.7	
CHO–BH$_3$ **7**	Cp	43.1	−7.6	35.4	13.0
	Et	8.3	−30.7	−22.4	
Standard deviation	Cp	4.8	13.9	18.7	
	Et	21.3	5.0	25.9	

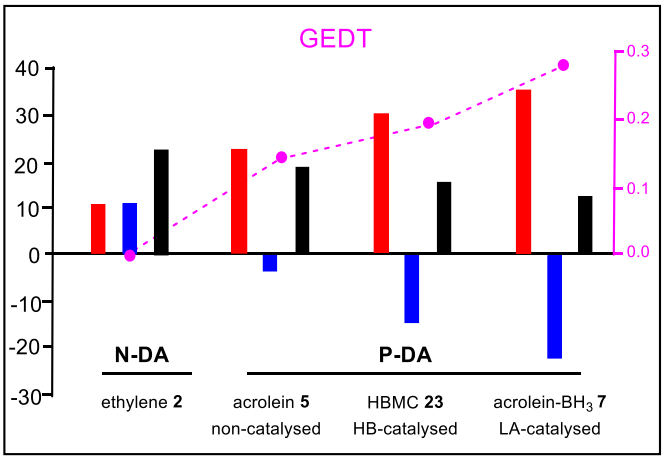

Fig. 10. Graphical representation of the sets of relative $E_{tot}(Cp)$ (in red), $E_{tot}(Et)$ (in blue), and $E_{tot}(Cp + Et)$ (in black) energies for the TSs associated with the four selected DA reactions of Cp **4** with ethylenes of increased electrophilic character. $E_{tot}(Cp + Et)$ corresponds to the activation energies of the reactions. The GEDT values at the TSs are plotted in pink. E(X) energies are given in kcal·mol^{-1}, and the GEDT in average number of electrons, e.

at the polar TSs is the main factor responsible for the decrease of the activation energies of these P-DA reactions (see the standard deviations of $E_{intra}(Et)$ in Table 5). As shown in Fig. 11, a very good linear correlation can be established between the decrease of the unfavorable relative $E_{intra}(Et)$ energies in the ethylene IQF and the GEDT that takes place in these DA reactions of FEDF, $R^2 = 0.97$; i.e., the higher the GEDT, the higher the intra-atomic stabilization of the ethylene framework and the faster the DA reaction. This finding is fully consistent with Parr's definition of the electrophilicity ω index, which accounts for the electronic stabilization of a species when it acquires a certain amount of electron density from the environment [9].

Consequently, the strong intra-atomic stabilization of the electrophilic ethylene IQF with the increase of the GEDT at the polar TSs, resulting from the HB formation, clarifies the pivotal role of the former in the decrease of the activation energies associated with these HB-catalysed P-DA reactions [8].

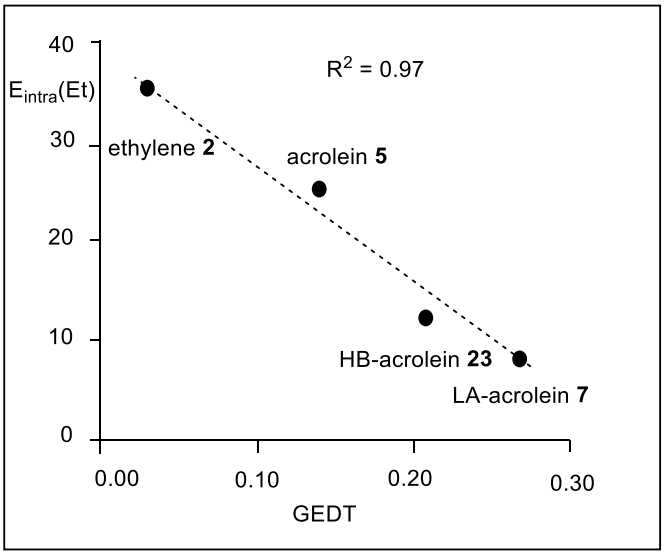

Fig. 11. Plot of the gas-phase B3LYP/6-311G(d,p) relative $E_{intra}(Et)$ energies of the ethylene framework (in kcal·mol^{-1}) versus the GEDT (in average number of electrons, e) for the DA reactions of Cp **4** with the four ethylenes of increased electrophilic character.

In order to identify the intrinsic electronic factors determining the activation energies of these HB catalysed DA reaction, a topological REG energy partitioning analysis was performed along the *endo* activation energy paths of the non-catalysed and catalysed DA reactions of Cp **4** with acrolein **5** and HBMC **18** (Acr:urea). A brief theoretical background on REG-IQA is given in the Computational Methods in Supplementary Material. The IQA terms with the largest REG values, expressed as ratios for comparative purposes (see the theoretical background), are given in Table 6, while Pearson correlation coefficients *R* are given in Table S9 in Supplementary Material.

The IQA-REG analysis shows a very similar energetic pattern for both P-DA reactions. In both cases, the two terms most contributing to the barrier are $V_{xc}(C5,C6)$ and $V_{xc}(C3,C4)$, followed by $V_{xc}(C1,C2)$ with a lower relative ratio of ca. 0.7. These three exchange-correlation V_{xc}^{AB} energy terms are associated with the covalent interactions, i.e. bonding changes, in the three C–C multiple bond regions of the reagents. Thus, these results indicate that the rupture of the C5–C6 and C3–C4 double bonds of acrolein **5** and Cp **4**, respectively, are the main factors responsible for the activation energies, followed by the more delayed depopulation of the C1–C2 double bond of Cp **4**. This agrees with the non-symmetric bonding changes observed from the BET study (see Section 4 in Supplementary Material). Note that the two reactions are highly asynchronous. On the other hand, the terms most working against the barrier, i.e. with negative REG values, are $V_{xc}(C4,C5)$, $V_{xc}(C2,C3)$, and $V_{xc}(C1,C6)$, which are associated with the favourable gathering of electron density in the C4–C5, C2–C3 and C1–C6 regions that will lead to the formation of the new single bonds between the Cp and acrolein moieties and to the formation of the C2=C3 double bond of the final CA **20** along the deactivation energy path. The ratios greater than −1 of $V_{xc}(C4,C5)$ account for the driving force of the two reactions, related to the formation of the first C4–C5 single bond. Indeed, these ratios also predict the higher bond formation asynchronicity in the HB-catalysed reaction.

Interestingly, the $V_{xc}(C6,C7)$ term, associated with the covalent bonding changes in the conjugated C6–C7 region of acrolein **5**, presents a negative REG value in both reactions. This confirms that the progressive accumulation of electron density observed in that region until reaching the TSs favours both reactions, i.e., works against the barrier. The most noticeable difference between both REG-IQA analyses is precisely the significantly higher contribution of that effect in lowering the activation energy of the HB-catalysed reaction; while $V_{xc}(C6,C7)$ has a ratio of −0.22 in the urea-promoted reaction, the ratio decreases to −0.14 when urea **16** is not present. Therefore, the unfavorable electrostatic interactions between the carbonyl C7 carbon and O8 oxygen, which have a negligible ratio of 0.11 in the non-catalysed reaction, have a greater weight in the barrier of the catalysed process, 0.25.

Table 6
Twelve largest REG_i values corresponding to the full IQA partitioning along the activation IRC path associated with the polar DA reactions of Cp **4** with acrolein **5** and HBMC **18**, involving urea **16** as HB catalyst. Ratios are defined as a given REG value divided by the largest positive REG value for the same considered reaction.

Non-catalysed			HB-catalysed		
Term	REG	Ratio	Term	REG	Ratio
$V_{xc}(C5,C6)$	2.71	1.00	$V_{xc}(C5,C6)$	3.15	1.00
$V_{xc}(C3,C4)$	2.53	0.93	$V_{xc}(C3,C4)$	2.96	0.94
$V_{xc}(C1,C2)$	1.92	0.71	$V_{xc}(C1,C2)$	2.05	0.65
$E_{intra}(C5)$	0.65	0.24	$V_{cl}(C7,O8)$	0.78	0.25
$E_{intra}(C4)$	0.62	0.23	$E_{intra}(C5)$	0.74	0.23
$E_{intra}(C0)$	0.44	0.16	$E_{intra}(C4)$	0.71	0.23
$V_{xc}(C6,C7)$	−0.39	−0.14	$E_{intra}(C7)$	−0.61	−0.19
$V_{cl}(C3,C4)$	−0.49	−0.18	$V_{cl}(C5,C6)$	−0.65	−0.21
$V_{cl}(C5,C6)$	−0.55	−0.20	$V_{xc}(C6,C7)$	−0.69	−0.22
$V_{xc}(C1,C6)$	−1.37	−0.50	$V_{xc}(C1,C6)$	−1.30	−0.41
$V_{xc}(C2,C3)$	−1.85	−0.68	$V_{xc}(C2,C3)$	−2.06	−0.65
$V_{xc}(C4,C5)$	−2.92	−1.08	$V_{xc}(C4,C5)$	−3.58	−1.13

Table 7
Variation, in kcal·mol^{-1}, of the most relevant V_{xc}^{AB} energy terms and of the total IQA energies of the Cp and acrolein moieties, from the first structure of the reaction path to the TS. The six terms with the highest positive and negative REG values are represented using coloured arrows. Labels indicate regions of the chemical structure. Label 'Ea' corresponds to the activation energy with respect to the first structure of the reaction path, while 'other' refers to the sum of the energies of every other full-partitioned IQA energy terms contributing towards or against the barrier. While the relative size of the coloured arrows is accurate, arrows in grey are only an approximation, indicated by the dashed top line.

	Non-catalysed	HB-catalysed
Region	ΔV_{xc}^{AB}	ΔV_{xc}^{AB}
C3–C4	56.4	58.1
C2–C3	−41.1	−40.2
C1–C2	42.6	40.4
C5–C6	60.7	61.9
C6–C7	−8.1	−13.2
C7–O8	4.2	7.1
C4–C5	−66.5	−71.3
C1–C6	−30.7	−25.8
IQA (Cp **4**)	21.8	27.9
IQA (acrolein **5**)	−2.7	−9.7

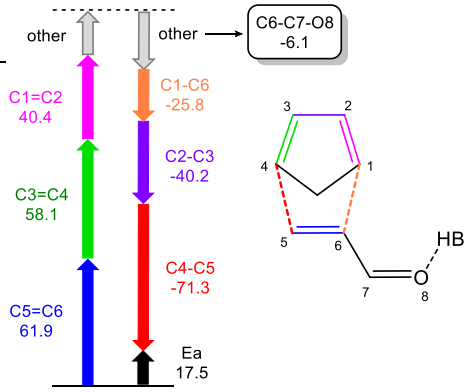

In order to quantify the energy costs of the most relevant bonding changes, the energy differences from reagents to TSs of the full-partitioned IQA terms with higher REG values are given in Table 7. Data show that while the rupture of the two C3–C4 and C5–C6 double bonds and formation of the C4–C5 and C1–C6 single bonds are slightly more unfavorable in the HB-catalysed reaction by 2.9 and 0.1 kcal mol^{-1}, respectively, the conjugation in the C6–C7–O8 region is more stabilizing by −2.2 kcal mol^{-1} as a consequence of the HBs between the oxygen of acrolein **5** and urea **16**. These HBs increase the global electrophilicity of acrolein from 1.84 to 2.58 eV and, therefore, the GEDT from 0.15 to 0.20 e.

In a polar reaction, the GEDT destabilizes the nucleophile and stabilizes the electrophile. In this case, when the REG-IQA is performed at the lowest atomic resolution, the total IQA energy of each molecular fragment shows that acrolein is stabilized and Cp is destabilized by, respectively, 7.0 and 6.1 kcal mol^{-1} more in the HB-catalysed process (see Table 7). Consequently, the HB interactions cause a higher stabilization of the acrolein moiety through the GEDT, and a more favourable conjugation of the received electron density, which explains the lower barrier by 2.0 kcal mol^{-1} of the HB-catalysed process. These HBs, which have an average covalent-bond strength of 6.1 kcal mol^{-1} according to the V_{xc}(O,H) energies at the starting structure of the activation energy path, become stronger by an average of 0.9 kcal mol^{-1} at the TS as the GEDT increases from reagents to the TS.

3. Conclusions

The role of HB formation in the P-DA reactions of Cp **4** with electrophilic acrolein **5** has been investigated within the MEDT at the ωB97X-D/6-311G(d,p) computational level by using a series of representative mono and bifunctional HB donor molecules.

ELF topological analysis of the electronic structure of HBMCs indicates that formation of one or two HBs with the carbonyl oxygen of acrolein **5** does not noticeably modify the GS electronic structure of this α,β-unsaturated aldehyde. Analysis of reactivity indices of the HBMCs shows that the formation of the HBs increases the electrophilicity ω index of these species, suggesting an acceleration of the DA reactions through more polar TSs, via FEDF processes. Analysis of the electrophilic Parr functions indicates that the β-conjugated carbon of the α,β-unsaturated aldehyde **5** is the most electrophilic centre of the HBMCs, thus determining the asynchronicity of these P-DA reactions.

Formation of one or two HBs with acrolein **5** decreases the activation energies of the HB-catalysed DA reactions by between 1.7 (methanol) and 4.0 (squaramide) kcal mol^{-1}, the corresponding P-DA reactions being low *endo* stereoselective. A clear correlation between the decrease of the activation energy of the HB-catalysed DA reactions and the GEDT taking place at the TSs is established; the stronger the HB interaction, the more polar and faster the P-DA reaction.

These DA reactions proceed through a non-concerted one-step mechanism via asynchronous C–C single bond formation processes, whose asynchronicity increases with the polar nature of the reaction. ELF and QTAIM topological analyses of the electron density at the TSs indicate that the formation of neither of the two C–C single bonds has started at any TS yet.

A rigorous IQA-IQF energy partitioning analysis of the TSs of P-DA reactions indicates that the intra-atomic stabilization of the acrolein framework as GEDT increases plays a crucial role in the decrease of the activation energies associated with these HB-catalysed DA reactions.

Supplementary Material: Computational Details. Study of the P-DA reaction between Cp **4** and acrolein **5**. Study of the fully optimized reaction paths associated with the HB-catalysed DA reactions of Cp **4** with acrolein **5** in the presence of bifunctionalised urea **16**, thiourea **17**, and squaramide **25**. BET study of the molecular mechanism of the DA reactions of Cp **4** with acrolein **5**, and with HBMC **18**. References. Fig. S8 includes ωB97X-D/6-311G(d,p) gas phase geometries of HBMCs **18**, **19** and **26**. Fig. S9 shows the *endo* and *exo* stereoisomeric TSs **TSn-19** and **TSx-19**. Table S5 displays the AIM parameters of the (3,-1) bonding CPs at HBMCs **6**, **18**, **24**, and **26** in the regions associated with the O–H HBs. Table S6 includes the ωB97X-D/6-311G(d,p) total electronic energies of the stationary points involved in the P-DA reactions of Cp **4** with HBMCs **6**, **18**, **19**, **22**–**24** and **26**. Table S7 involves the ωB97X-D/6-311G(d,p) total and relative energies with respect to the separated reagents, in water, of the stationary points involved in the DA reaction of Cp **4** with acrolein **5**, and with HBMC **26**. Table S8 includes the AIM parameters of (3,-1) bonding CPs at **TSn-6**, **TSn-18** and **TSn-24**, in the regions associated with the C–C single bond formation, **CP1** and **CP2**, and with the O–H HBs, **CP3** and **CP4**. Table S9 contains Pearson correlation coefficients R of the twelve fully-partitioned IQA terms with largest REG_i values along the activation IRC paths associated with the P-DA reactions of Cp **4** with acrolein **5**, and with HBMC **18**. ωB97XD/6-311G(d,p) gas phase computed total energies and Cartesian coordinates of the stationary points involved in the P-DA reactions between Cp **4** and acrolein **5**, and with HBMCs **6**, **18**, **19**, **22**–**24** and **26**.

CRediT authorship contribution statement

Luis R. Domingo: Writing – review & editing, Writing – original draft, Supervision, Project administration, Investigation, Conceptualization. **Patricia Pérez:** Writing – review & editing, Writing – original draft, Investigation. **Mar Ríos-Gutiérrez:** Writing – review & editing, Writing – original draft, Methodology, Investigation. **M. José Aurell:** Writing – review & editing, Writing – original draft, Investigation.

Declaration of competing interest

The authors declare that they have no known competing financial interests or personal relationships that could have appeared to influence the work reported in this paper.

Data availability

Data will be made available on request.

Acknowledgments

This work has been supported by the Ministry of Science and Innovation (MICINN) of the Spanish Government, project PID2019-110776 GB-I00 (AEI/FEDER, UE) and by FONDECYT - Chile through Project No. 1221383. L.R.D. also acknowledges Cooperación Internacional (Fondecyt No. 1221383) by continuous support.

Appendix A. Supplementary data

Supplementary data to this article can be found online at https://doi.org/10.1016/j.tchem.2024.100064.

References

[1] O. Diels, K. Alder, Ann. Chem. 460 (1928) 98–122.
[2] W. Carruthers, in: Some Modern Methods of Organic Synthesis, second ed., Cambridge University Press, Cambridge, 1978.
[3] W. Carruthers, in: Cycloaddition Reactions in Organic Synthesis, Pergamon, Oxford, 1990.
[4] F.A. Carey, R.J. Sundberg, in: Advanced Organic Chemistry. Part A: Strucutre and Mechanisms, fifth ed., Springer, New York, 2007.
[5] R.B. Woodward, R. Hoffmann, Angew Chem. Int. Ed. Engl. 8 (1969) 781–853.
[6] D. Rowley, H. Steiner, Discuss. Faraday Soc. 10 (1951) 198–213.
[7] L.R. Domingo, RSC Adv. 4 (2014) 32415–32428.
[8] L.R. Domingo, J.A. Sáez, Org. Biomol. Chem. 7 (2009) 3576–3583.
[9] R.G. Parr, L. von Szentpaly, S. Liu, J. Am. Chem. Soc. 121 (1999) 1922–1924.
[10] L.R. Domingo, E. Chamorro, P. Pérez, J. Org. Chem. 73 (2008) 4615–4624.
[11] L.R. Domingo, M. Ríos-Gutiérrez, P. Pérez, Molecules 21 (2016) 748.
[12] L.R. Domingo, M. Ríos-Gutiérrez, in: Shubin Liu (Ed.), Application of Reactivity Indices in the Study of Polar Diels–Alder Reactions. Conceptual Density Functional Theory: towards a New Chemical Reactivity Theory, vol. 2, WILEY-VCH GmbH, 2022, pp. 481–502.
[13] L.R. Domingo, M. Ríos-Gutiérrez, P. Pérez, Molecules 25 (2020) 2535.
[14] W.L. Jorgensen, J.F. Blake, D. Lim, D. Severance, J. Chem. Soc. Faraday. Trans. 90 (1994) 1727–1732.
[15] Y. Huang, V.H. Rawal, J. Am. Chem. Soc. 124 (2002) 9662–9663.
[16] L.R. Domingo, J. Andrés, J. Org. Chem. 68 (2003) 8662–8668.
[17] P. Vermeeren, T.A. Hamlin, F.M. Bickelhaupt, I. Fernández, Chem. Eur J. 27 (2021) 5180–5190.
[18] F.M. Bickelhaupt, J. Comput. Chem. 20 (1999) 114–128.
[19] D.M. Andrada, C. Foroutan-Nejad, Phys. Chem. Chem. Phys. 22 (2020) 22459–22464.
[20] J. Poater, D.M. Andrada, M. Solà, C. Foroutan-Nejad, Phys. Chem. Chem. Phys. 24 (2022) 2344–2348.
[21] R.F.W. Bader, Chem. Eur J. 12 (2006) 2896–2901.
[22] L.R. Domingo, Molecules 21 (2016) 1319.
[23] K. Fukui, in: Molecular Orbitals in Chemistry, Physics, and Biology, New York, 1964.
[24] R.D. Froese, J.M. Coxon, S.C. West, K. Morokuma, J. Org. Chem. 62 (1997) 6991–6996.
[25] K. Morokuma, K. Kitaura, in: Chemical Applications of Atomic and Molecular Electrostatic Potentials, Plenum, New York, 1981, pp. 215–242.
[26] R.G. Parr, W. Yang, Density Functional Theory of Atoms and Molecules, Oxford University Press, New York, 1989.
[27] A.D. Becke, K.E. Edgecombe, J. Chem. Phys. 92 (1990) 5397–5403.
[28] K. Krokidis, S. Noury, B. Silvi, J. Phys. Chem. A 101 (1997), 7277−7282.
[29] R.F.W. Bader, Y.H. Tang, Y. Tal, F.W. Biegler-König, J. Am. Chem. Soc. 104 (1982) 946–952.
[30] R.F.W. Bader, Atoms in Molecules: A Quantum Theory, Oxford University Press, Oxford, New York, 1994.
[31] E.R. Johnson, S. Keinan, P. Mori-Sanchez, J. Contreras-Garcia, J. Cohen, W. Yang, J. Am. Chem. Soc. 132 (2010) 6498–6506.
[32] M.A. Blanco, A. Martín Pendás, E. Francisco, J. Chem. Theor. Comput. 1 (2005) 1096–1109.
[33] J.C.R. Thacker, P.L.A. Popelier, Theor. Chem. Acc. 136 (2017) 86.
[34] I. Alkorta, A.F. Silva, P.L.A. Popelier, Molecules 25 (2020) 2674.
[35] J.C.R. Thacker, P.L.A. Popelier, J. Phys. Chem. A 122 (2018) 1439–1450.
[36] M. Ríos-Gutiérrez, F. Falcioni, L.R. Domingo, P.L.A. Popelier, Phys. Chem. Chem. Phys. 25 (2023) 10853–10865.
[37] B. Silvi, A. Savin, Nature 371 (1994) 683–686.
[38] A.E. Reed, R.B. Weinstock, F. Weinhold, J. Chem. Phys. 83 (1985) 735–746.
[39] A.E. Reed, L.A. Curtiss, F. Weinhold, Chem. Rev. 88 (1988) 899–926.
[40] E. Espinosa, I. Alkorta, J. Elguero, E. Molins, J. Chem. Phys. 117 (2002) 5529–5542.
[41] R.G. Parr, R.G. Pearson, J. Am. Chem. Soc. 105 (1983) 7512–7516.
[42] L.R. Domingo, M. Ríos-Gutiérrez, P. Pérez, RSC Adv. 10 (2020) 15394–15405.
[43] L.R. Domingo, M. Ríos-Gutiérrez, Sci. Rad. 2 (2023) 1.
[44] L.R. Domingo, P. Pérez, J.A. Sáez, RSC Adv. 3 (2013) 1486–1494.
[45] L.R. Domingo, M.J. Aurell, P. Pérez, J.A. Sáez, RSC Adv. 2 (2012) 1334–1342.
[46] J. Andrés, V. Moliner, J. Krech, E. Silla, J. Chem. Soc. Perkin Trans. 2 (1995) 1551–1558.
[47] R. Cárdenas, J. Andrés, J. Krechl, M. Campillo, O. Tapias, Int. J. Quant. Chem. 57 (1996) 245–257.
[48] P.R. Schreiner, A. Wittkopp, Org. Lett. 4 (2002) 217–220.
[49] A. Wittkopp, P.R. Schreiner, Chem. Eur J. 9 (2003) 407–414.
[50] L.R. Domingo, M. Ríos-Gutiérrez, P. Pérez, Tetrahedron 73 (2017) 1718–1724.
[51] J.A. Rackers, J.W. Ponder, J. Chem. Phys. 150 (2019) 084104.
[52] R. Gleiter, M.C. Bohm, Pure Appl. Chem. 55 (1983) 237–244.
[53] L.R. Domingo, M. Arnó, J. Andrés, J. Org. Chem. 64 (1999) 5867–5875.
[54] J.I. García, J.A. Mayoral, L. Salvatella, Acc. Chem. Res. 33 (2000) 658–664.
[55] L.R. Domingo, J.A. Sáez, J. Org. Chem. 76 (2011) 373–379.
[56] L.R. Domingo, J.A. Sáez, R.J. Zaragozá, M. Arnó, J. Org. Chem. 73 (2008) 8791–8799.
[57] L. Triestram, F. Falcioni, P.L.A. Popelier, ACS Omega 8 (2023) 34844–34851.
[58] J.C.R. Thacker, P.L.A. Popelier, Theor. Chem. Acc. 136 (2017) 86.